Evaporation residue cross-section measurements for ^{48}Ti-induced reactions

Priya Sharma,* B. R. Behera,† Ruchi Mahajan, Meenu Thakur, Gurpreet Kaur, Kushal Kapoor, and Kavita Rani
Department of Physics, Panjab University, Chandigarh 160014, India

N. Madhavan, S. Nath, J. Gehlot, and R. Dubey
Inter University Accelerator Centre, Aruna Asaf Ali Marg, New Delhi 110067, India

I. Mazumdar and S. M. Patel
Tata Institute of Fundamental Research, Mumbai 400005, India

M. Dhibar
Department of Physics, Indian Institute of Technology, Roorkee 247667, India

M. M. Hosamani
Department of Physics, Karnatak University, Dharwad 580003, India

Khushboo and Neeraj Kumar
Department of Physics and Astrophysics, University of Delhi 110007, India

A. Shamlath
Department of Physics, Central University of Kerala, Kasaragod 671314, India

G. Mohanto
Nuclear Physics Division, Bhabha Atomic Research Centre, Mumbai 400085, India

Santanu Pal‡
CS-6/1 Golf Green, Kolkata 700095, India

(Received 5 March 2017; revised manuscript received 22 June 2017; published 20 September 2017)

Background: A significant research effort is currently aimed at understanding the synthesis of heavy elements. For this purpose, heavy ion induced fusion reactions are used and various experimental observations have indicated the influence of shell and deformation effects in the compound nucleus (CN) formation. There is a need to understand these two effects.
Purpose: To investigate the effect of proton shell closure and deformation through the comparison of evaporation residue (ER) cross sections for the systems involving heavy compound nuclei around the $Z_{CN} = 82$ region.
Methods: A systematic study of ER cross-section measurements was carried out for the ^{48}Ti + ^{142,150}Nd, ^{144}Sm systems in the energy range of 140–205 MeV. The measurement has been performed using the gas-filled mode of the hybrid recoil mass analyzer present at the Inter University Accelerator Centre (IUAC), New Delhi. Theoretical calculations based on a statistical model were carried out incorporating an adjustable barrier scaling factor to fit the experimental ER cross section. Coupled-channel calculations were also performed using the CCFULL code to obtain the spin distribution of the CN, which was used as an input in the calculations.
Results: Experimental ER cross sections for ^{48}Ti + ^{142,150}Nd were found to be considerably smaller than the statistical model predictions whereas experimental and statistical model predictions for ^{48}Ti + ^{144}Sm were of comparable magnitudes.
Conclusion: Though comparison of experimental ER cross sections with statistical model predictions indicate considerable non-compound-nuclear processes for ^{48}Ti + ^{142,150}Nd reactions, no such evidence is found for the ^{48}Ti + ^{144}Sm system. Further investigations are required to understand the difference in fusion probabilities of ^{48}Ti + ^{142}Nd and ^{48}Ti + ^{144}Sm systems.

DOI: 10.1103/PhysRevC.96.034613

I. INTRODUCTION

In recent years, a great deal of experimental as well as theoretical work has been carried out in order to understand the fusion-fission reactions leading to heavy element formation. The fusion of nuclei is governed by a delicate balance between the attractive nuclear and repulsive Coulomb interactions,

*priya.apr25@gmail.com
†Corresponding author: bivash@pu.ac.in
‡Formerly with VECC, Kolkata.

TABLE I. Parameters of the studied projectile-target combinations.

Systems	β_2		E_{2^+} (MeV)		V_b	Q value	Fissility	Entrance-channel
	Projectile	Target	Projectile	Target	(MeV)	(MeV)	(χ)	mass asymmetry (α)
^{48}Ti + ^{142}Nd	0.27	0.092	0.98	1.57	153.39	−114.03	0.72	0.49
^{48}Ti + ^{150}Nd	0.27	0.280	0.98	0.13	151.74	−96.13	0.70	0.52
^{48}Ti + ^{144}Sm	0.27	0.088	0.98	1.66	158.07	−122.39	0.74	0.50

influenced by the presence of coupling to various internal degrees of freedom [1,2]. In the formation of heavy elements, a particular selection of the projectile and the target (light or heavy) plays a crucial role. Heavy ion induced reactions offer a wide range of possibilities for heavy element formation. The detailed study of heavy element and super-heavy element (SHE) formation involves the compound nucleus (CN) decay product, i.e., evaporation residue (ERs) [3–6] whose formation probability is suppressed not only by fusion-fission (CN fission fragments [7,8]), but also by non-compound-nuclear (NCN) processes, i.e., quasifission (QF) (reseparation before CN formation [9–11]). Near the Coulomb barrier energies, fusion-fission and QF exhibit their own characteristic reaction times. ERs carry the true signatures of CN formation and are a useful probe to study the statistical as well as the dynamical aspects of the fusion-fission reactions. The main difficulty in forming a nucleus in the SHE region is its extremely low production rate (cross section of the order ∼pb). The onset of QF is a major hurdle in the formation of SHE and a growing number of experiments are reporting the presence of the QF process [7,12,13]. Some of the experimental signatures of the QF process are anomalous fission fragment angular anisotropies [14,15], broader fission fragment mass widths [16,17], and a reduction in ER cross section [18]. This latter can be attributed to the fact that the dinuclear system reseparates before the full shape equilibration of CN. These measurements are predicted to be dependent on the entrance-channel properties like energy, entrance-channel mass asymmetry [19], deformation and relative orientation [9,20], fissility value [21,22], and shell effects [23,24] of the colliding nuclei. It thus becomes important to understand such processes and to know to what extent entrance-channel properties contribute to the stability of a heavy nucleus against fission in heavy and super-heavy regions.

It is established that the fusion cross section is significantly reduced even for very asymmetric reactions due to the presence of QF. Berriman *et al.* studied ^{12}C + ^{204}Pb, ^{19}F + ^{197}Au, and ^{30}Si + ^{186}W systems, all forming the same CN ^{216}Ra* [18], and concluded that the fusion hindrance was strongly dependent on the mass asymmetry of the entrance channel and related to the onset of the QF process. Back *et al.* [19] measured full angular distribution for the three systems, leading to the same CN ^{214}Th*. Evidence for QF was found for ^{32}S + ^{182}W and complete fusion was only a small fraction of the total reaction cross section for ^{48}Ti + ^{166}Er and ^{60}Ni + ^{154}Sm systems. In an another work, Sagaidak *et al.* [25] observed a sizable contribution of QF through the ER and fission cross-section measurements for more symmetric ^{48}Ca + ^{168,170}Er systems (ER cross section indicates 70% suppression of the CN formation) in comparison to asymmetric ^{12}C + ^{204,206,208}Pb systems. For a number of systems, enhancement of fission width is achieved by reducing the height of the liquid drop model (LDM) fission barrier [25,26] in order to fit the ER and fission excitation functions in the framework of the standard statistical model. Knyazheva *et al.* [7] have found that the QF effect is more prominent with the beam and target combination ^{48}Ca + ^{154}Sm, which corresponds to a greater value for the entrance-channel mass asymmetry than ^{48}Ca + ^{144}Sm, where ^{154}Sm is a deformed and ^{144}Sm is a spherical nucleus in their ground state. The synthesis of elements with mass numbers 114 [27] and 116 [28] using a ^{48}Ca beam on ^{244}Pu and ^{248}Cm targets (well-deformed nuclei) indicates that shell stabilization close to the next higher proton shell could favor the synthesis of heavy nuclei [29].

Keeping the above points in mind, a systematic measurement of ER cross sections was carried out for understanding the reaction mechanism involving heavy compound nuclei of (i) ^{48}Ti + ^{142}Nd → ^{190}Pb*, (ii) ^{48}Ti + ^{150}Nd → ^{198}Pb*, and (iii) ^{48}Ti + ^{144}Sm → ^{192}Po* systems leading to compound nuclei around the $Z_{CN} = 82$ region. Here, the target ^{142}Nd ($\beta_2 = 0.092$) is spherical and ^{150}Nd is deformed ($\beta_2 = 0.28$) in their ground states. In the third system, the target ^{144}Sm ($\beta_2 = 0.088$) is also spherical; however, it leads to ^{192}Po* CN ($Z_{CN} = 84$), which has two extra protons beyond the proton shell closure ($Z_{CN} = 82$). Various other parameters related to the studied projectile-target combinations are given in Table I. The effect of proton shell closure and deformation can be disentangled through the comparison of ER cross sections of these three systems. It is also of interest to study if there is any enhanced survival probability for ER cross sections in the $Z_{CN} = 82$ region. Theoretical calculations were performed using the statistical model of CN decay where shell effects are considered in both the level density and fission barrier.

The paper is organized as follows. Experimental details are given in the next section. Section III explains the data analysis and transmission efficiency calculations to evaluate the ER cross sections. Theoretical calculations are presented in Sec. IV with discussion in Sec. V, and finally, the last section contains the summary and conclusions.

II. EXPERIMENTAL DETAILS

The experiment was performed at the beam-hall II of IUAC using 15UD Pelletron + LINAC accelerator facility. Thin isotopically enriched targets ^{142,150}Nd (enrichment = 98.26% and 96.11%; thickness = 100 and 150 μg/cm^2, respectively) and ^{144}Sm (enrichment = 93.70% and thickness = 120 μg/cm^2) sandwiched [30] between two very thin carbon

layers (25 and 7 μg/cm^2) were used in the experiment. ER cross-section measurements were carried out using a pulsed ^{48}Ti beam with 1 μs pulse separation at energies in the center of mass ranging from 140 to 205 MeV (including energy loss from 650 μg/cm^2 carbon window foil, carbon backing, and a half thickness of targets ~17 MeV) with an average current of 0.5 pnA.

The heavy ERs formed in the experiment were separated from the enormous beam background using the gas-filled mode of hybrid recoil mass analyzer (HYRA) [31] present at IUAC, New Delhi. The gas-filled region of HYRA was isolated from the vacuum region using 650 μg/cm^2 carbon window foil. In the present experiment, He gas was used in HYRA for velocity and charge state focusing of the ions. Pressure scanning was performed at different pressures (0.20, 0.25, 0.30, and 0.35 Torr) and the ratio of ER and monitor counts (known as yield) was found to be maximum at 0.30 Torr. Hence, in the whole experiment He gas pressure was fixed at the optimized value of 0.30 Torr. The electromagnetic configuration of the HYRA is Q_1Q_2-MD_1-Q_3-MD_2-Q_4Q_5 where the Q stands for the magnetic quadrupole and MD stands for the magnetic dipole. The value of the fields was calculated using a simulation program [32]. For the field optimization, the field scanning was performed in the ±10% in steps of 2% from the calculated values at each energy point.

Two silicon surface barrier detectors (SSBDs) were placed inside the target chamber at a distance of 45 mm from the target ladder subtended an angle of ±25° with respect to the beam direction. SSBD (known as a monitor) collected elastically scattered Ti ions which were used for Rutherford cross-section normalization. Monitor detectors were also used for the beam positioning at the center of the target. ER counts were detected using a position sensitive multiwire proportional counter (MWPC) of dimensions 6 × 2 in^2 followed by a strip detector of dimensions 6 × 6 cm^2 kept in the focal plane chamber. In the present experiment, MWPC counts were used for the measurement of the ER cross section. The detector was operated with isobutane gas at 1.5 mbar pressure and provided position (X_L, X_R, Y_U, and Y_D) signals, energy loss signal (cathode), and timing signal (anode).

The position signals (acting as the stop signal) were processed by a constant fraction discriminator (CFD) and then fed to a time-to-digital converter (TDC) using the anode signal as a common start. Energy (MWPC cathode and monitors) signals were fed to an analog-to-digital converter (ADC) for further processing. The logical 'OR' signal of monitors and MWPC anode acted as a master strobe for the data acquisition system. ERs were detected by the time-of-flight (TOF) technique, hence, to extract a TOF spectrum, an anode (timing) signal was used as a stop and rf of the beam as a start signal. Data were collected and analyzed using the IUAC data-sorting software CANDLE [33]. The details about the data analysis are given in the next section.

III. DATA ANALYSIS

A. ER cross-section measurements

The formula to calculate the total ER cross section is given by

$$\sigma_{ER} = \left(\frac{Y_{ER}}{Y_{Mon}}\right)\left(\frac{d\sigma}{d\Omega}\right)_R \Omega_{Mon}\frac{1}{\eta_{HYRA}}, \quad (1)$$

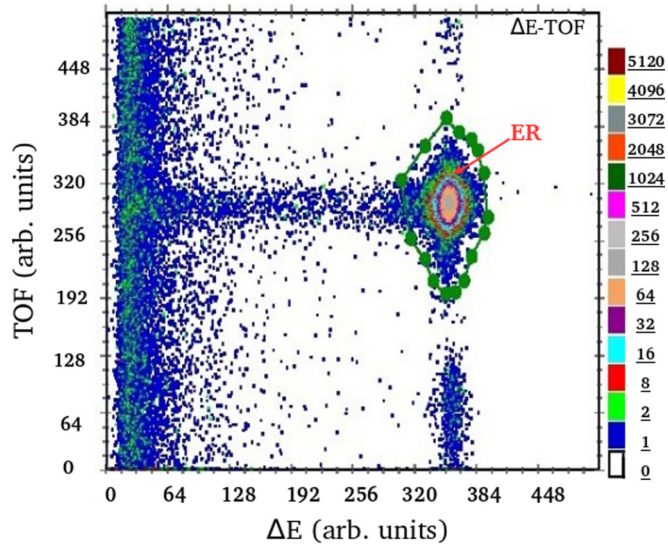

FIG. 1. Two-dimensional spectrum obtained from the TOF and energy loss (ΔE) signal for the ^{48}Ti + ^{150}Nd system at $E_{c.m.}$ = 157.83 MeV.

where σ_{ER} is the ER cross section in mb, Y_{ER} is the ER yield at the focal plane, Y_{Mon} is the average yield from both monitor detectors (left and right), Ω_{Mon} is the solid angle subtended by the monitor detectors, and η_{HYRA} is the HYRA transmission efficiency. To obtain the ER yield, a two-dimensional plot was generated using the TOF and energy loss (ΔE) signal of the MWPC which provides a clean separation of ERs. The ERs reaching the focal plane (shown in the two-dimensional gate) were well separated from the other contaminations as shown in Fig. 1.

The yield of monitor detectors was obtained from the one-dimensional single spectrum using the CANDLE software. The differential Rutherford scattering cross section is given by

$$\left(\frac{d\sigma}{d\Omega}\right)_R = 1.296\left(\frac{Z_pZ_t}{E_{lab}}\right)^2\left[\frac{1}{\sin^4\left(\frac{\theta}{2}\right)} - 2\left(\frac{A_p}{A_t}\right)^2\right], \quad (2)$$

where Z_p, Z_t and A_p, A_t are the atomic and mass numbers of the projectile and target, respectively. E_{lab} and θ are the energy of the incident projectile and scattering angle of the projectile-like particles in the laboratory frame of reference, respectively.

B. Transmission efficiency of ^{48}Ti + ^{142,150}Nd, ^{144}Sm systems

In the ER cross-section measurements, extraction of transmission efficiency plays a vital role. It is the ratio of the number of ERs reaching the focal plane to the total number of ERs produced in the target chamber and it depends on various parameters [3–6]. The η_{HYRA} is given by the formula

$$\eta_{HYRA} = \left(\frac{Y_{ER}}{Y_{Mon}}\right)\left(\frac{d\sigma}{d\Omega}\right)_R \Omega_{Mon}\frac{1}{\sigma_{ER}}, \quad (3)$$

In the literature, the experimental fusion cross section (ER and fission data) of the ^{48}Ti + ^{122}Sn system already exists [34,35]. Hence, the ^{48}Ti + ^{122}Sn system was used as a

TABLE II. η_{HYRA} for ^{48}Ti + ^{122}Sn calibration reaction.

$E_{\mathrm{c.m.}}$ (MeV)	$\eta_{\mathrm{HYRA}} \pm$ error (%)
146.68	34.86 ± 5.23
159.26	22.55 ± 3.38
Average efficiency	28.71 ± 4.31

calibration reaction in the efficiency measurement. Using the same experimental setup, measurements were carried out for the ^{48}Ti + ^{122}Sn system at 146.68 and 159.26 MeV (energies in center-of-mass frame). The η_{HYRA} for the ^{48}Ti + ^{122}Sn system was obtained from Eq. (3) and the η_{HYRA} at both the energy points are given in Table II. The experimentally extracted average transmission efficiency value for the ^{48}Ti + ^{122}Sn system is 28.71% ± 4.31% (Table II). This average efficiency value was used in the final calculations to determine the efficiency for the ^{48}Ti + ^{142,150}Nd, ^{144}Sm systems.

The ERs produced in the reactions should have sufficient amount of energy so that they can travel the path length of HYRA and reach the focal plane chamber. So, the energy loss of the ERs was taken into account through the calculation of energy loss in the half thickness of the target, He gas at 0.30 Torr, Mylar foil (separates the gas-filled region of HYRA from the focal plane chamber), and isobutane gas. Because the ^{48}Ti + ^{142,150}Nd, ^{144}Sm systems are more symmetric than the ^{48}Ti + ^{122}Sn system, the ER angular distribution of the former systems would be narrower than the latter system.

Next for calculating transmission efficiency of the recoil separator for our measured systems, the ER angular distributions for the three systems were simulated using the code TERS [36]. TERS is a semimicroscopic Monte Carlo simulation code, which takes the actual input parameters during the experiment like beam spot, target thickness, the gas pressure in the separator, and other parameters such as α, proton, neutron separation energy, etc. In the calculation the interaction of the beam with the target is treated event by event and in the output, it generates the realistic distribution of ERs such as divergence (angle), energy, and charge state in event-by-event mode. The statistical model code PACE3 [37] was used to obtain the various possible ER channels and their relative yields (used for normalization of the angular distribution) and the TERS code was used to calculate the angular distribution of individual ERs at each energy point. Here, energy and charge state acceptance was assumed nearly 100%; but in the present experiment, the acceptance angle is limited by the narrow aperture of the used target chamber, translating to a polar angle of 9.5°. Hence, the average area under the curve was considered up to 9.5° in the present calculations. The normalized angular distribution at each energy was obtained by adding the individual ER angular distribution with proper weighted yield and the obtained normalized distributions for the ^{48}Ti + ^{142,150}Nd, ^{144}Sm systems are shown in Fig. 2. A multiplication factor was obtained by the ratio of the area under the curve (using the ^{48}Ti + ^{122}Sn calibration reaction and ^{48}Ti + ^{142,150}Nd, ^{144}Sm systems) up to 9.5° and it was evaluated at each energy point. The average η_{HYRA} obtained from the ^{48}Ti + ^{122}Sn system was then multiplied with the subsequent multiplication factor and the efficiency values were extracted for the three systems in the measured energy range (mentioned in Table III). The efficiency values obtained in the present work are increasing with the increase in energy.

The difference in the behavior of angular distributions is clearly visible in the three reactions. In order to conclude further, we next performed statistical model calculations with a standard set of parameters for the three systems and obtained the angular distributions and relative yields of the different ER channels for these reactions. The angular distribution plot is shown in Fig. 3. The difference in angular distribution is the result of different particle emission and is clearly seen in Figs. 2 and 3. The proton and α evaporations become

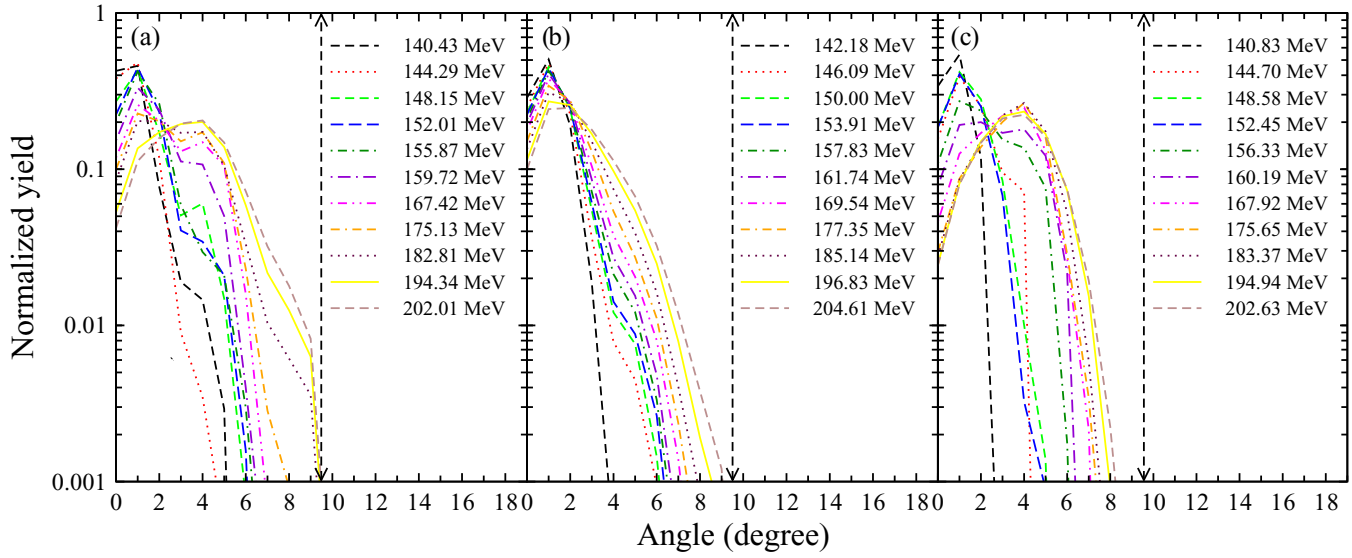

FIG. 2. Normalized angular distributions simulated by the TERS code for (a) ^{48}Ti + ^{142}Nd, (b) ^{48}Ti + ^{150}Nd, and (c) ^{48}Ti + ^{144}Sm systems at measured energy ranges. These distributions were compared with the ^{48}Ti + ^{122}Sn system to get the correction in η_{HYRA}. Angular acceptance of HYRA is 9.5° which is marked here by the vertical dashed line.

TABLE III. η_{HYRA} for ^{48}Ti + ^{142,150}Nd, ^{144}Sm systems as a function of $E_{\mathrm{c.m.}}$ and E^*.

^{48}Ti + ^{142}Nd			^{48}Ti + ^{150}Nd			^{48}Ti + ^{144}Sm		
$E_{\mathrm{c.m.}}$ (MeV)	E^* (MeV)	$\eta_{\mathrm{HYRA}} \pm$ error (%)	$E_{\mathrm{c.m.}}$ (MeV)	E^* (MeV)	$\eta_{\mathrm{HYRA}} \pm$ error (%)	$E_{\mathrm{c.m.}}$ (MeV)	E^* (MeV)	$\eta_{\mathrm{HYRA}} \pm$ error (%)
140.43	26.41	24.51 ± 3.68	142.18	46.06	26.68 ± 4.00	140.83	18.45	26.27 ± 3.94
144.29	30.27	25.21 ± 3.78	146.09	49.97	27.23 ± 4.08	144.70	22.32	28.10 ± 4.21
148.15	34.13	26.89 ± 4.03	150.00	53.88	27.56 ± 4.13	148.58	26.19	28.46 ± 4.27
152.01	37.98	27.66 ± 4.15	153.91	57.79	27.66 ± 4.15	152.45	30.07	28.82 ± 4.32
155.87	41.85	27.94 ± 4.19	157.83	61.71	27.86 ± 4.18	156.33	33.94	29.04 ± 4.36
159.72	45.70	28.71 ± 4.31	161.74	65.61	28.08 ± 4.21	160.19	37.81	29.49 ± 4.42
167.42	53.40	28.75 ± 4.31	169.54	73.42	28.28 ± 4.24	167.92	45.54	29.51 ± 4.43
175.13	61.10	29.29 ± 4.39	177.35	81.23	28.56 ± 4.28	175.65	53.27	30.66 ± 4.60
182.81	68.78	29.65 ± 4.45	185.14	89.02	29.02 ± 4.35	183.37	60.98	30.67 ± 4.60
194.34	80.31	30.12 ± 4.52	196.83	100.71	29.31 ± 4.40	194.94	72.55	30.69 ± 4.60
202.01	87.98	30.20 ± 4.53	204.61	108.49	29.51 ± 4.43	202.63	80.25	30.35 ± 4.55

increasingly important with increasing excitation energy of the CN. Therefore the recoil on the residual nucleus and hence the angular spread increases with increase of CN excitation energy. The angular distributions for the ^{48}Ti + ^{142}Nd, ^{144}Sm systems are broader as compared to ^{48}Ti + ^{150}Nd at a given beam energy as a larger number of α are emitted in the former two systems on account of their neutron deficiency.

C. Experimental results

The ER cross sections were extracted using the transmission efficiency values at each energy point which are mentioned in Table IV. The error in cross section was estimated from the error in η_{HYRA}, systematic error, and statistical error (obtained from the experimental parameters Y_{ER} and Y_{Mon}). The estimated error is 15% of the obtained cross sections for which the contribution from η_{HYRA} is maximum. The experimentally obtained ER cross sections as a function of $E_{\mathrm{c.m.}}$ for the ^{48}Ti + ^{142,150}Nd, ^{144}Sm systems are shown in Fig. 4.

Statistical model predictions with standard parameters do not reproduce the experimental ER cross sections as it would be subsequently found. To check the sensitivity of the ER angular distribution on ER (or fission) cross sections, a test calculation was made where fission was totally suppressed and the entire incident flux went to ER formation. The calculations were performed for two representative energies around 175 and 194 MeV c.m. energy for all three systems, in which we have actually taken the measurements. The results are compared in Fig. 5 where the effect of magnitude of the ER cross section on ER angular distribution is found to be marginal. Consequently, it establishes that the angular acceptance of the experimental setup is practically independent of the magnitude of the ER cross section. It may, however, be pointed out that with increasing ER cross section, more and more compound nuclei with higher spin become ER events. Consequently, the

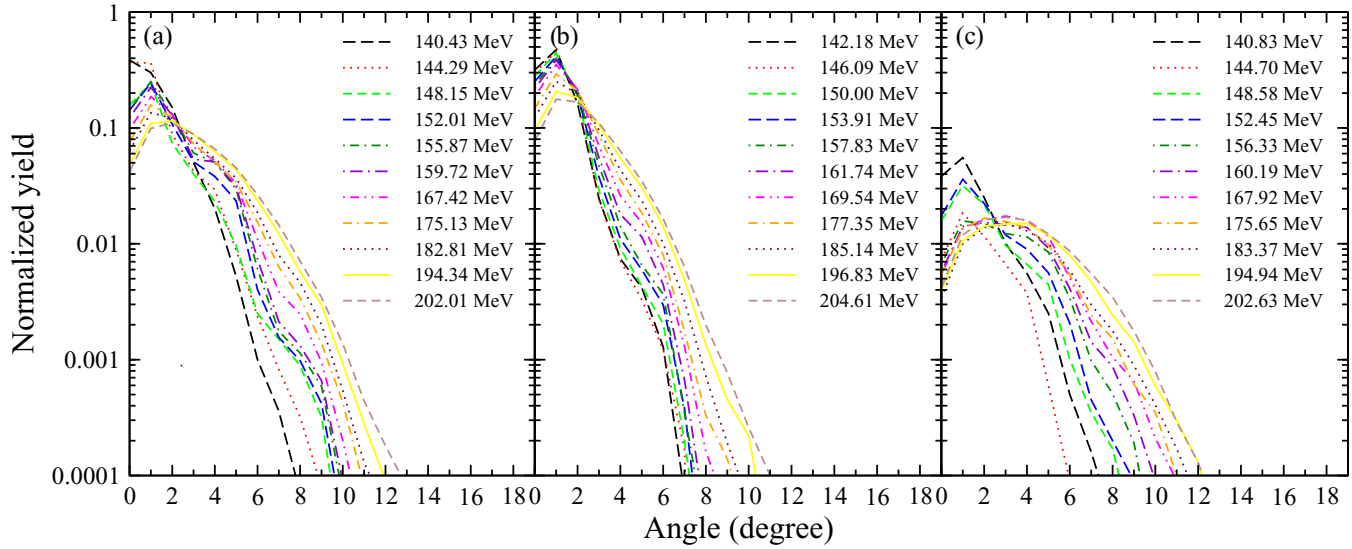

FIG. 3. Statistical model predictions for ER angular distribution of (a) ^{48}Ti + ^{142}Nd, (b) ^{48}Ti + ^{150}Nd, and (c) ^{48}Ti + ^{144}Sm systems.

TABLE IV. Measured σ_{ER} for $^{48}Ti + ^{142,150}Nd$, ^{144}Sm systems as a function of $E_{c.m.}$ and E^*.

$^{48}Ti + ^{142}Nd$			$^{48}Ti + ^{150}Nd$			$^{48}Ti + ^{144}Sm$		
$E_{c.m.}$ (MeV)	E^* (MeV)	$\sigma_{ER} \pm$ error (mb)	$E_{c.m.}$ (MeV)	E^* (MeV)	$\sigma_{ER} \pm$ error (mb)	$E_{c.m.}$ (MeV)	E^* (MeV)	$\sigma_{ER} \pm$ error (mb)
140.43	26.41	11.35 ± 1.72	142.18	46.06	4.74 ± 0.97	140.83	18.45	13.27 ± 2.01
144.29	30.27	12.70 ± 1.91	146.09	49.97	13.58 ± 2.04	144.70	22.32	17.89 ± 2.70
148.15	34.13	12.91 ± 1.95	150.00	53.88	31.39 ± 4.72	148.58	26.19	18.14 ± 2.74
152.01	37.98	12.01 ± 1.82	153.91	57.79	55.13 ± 8.29	152.45	30.07	15.87 ± 2.38
155.87	41.85	10.80 ± 1.64	157.83	61.71	63.97 ± 9.60	156.33	33.94	15.99 ± 2.44
159.72	45.70	11.80 ± 1.78	161.74	65.61	83.56 ± 12.59	160.19	37.81	14.93 ± 2.28
167.42	53.40	12.54 ± 2.52	169.54	73.42	78.85 ± 11.89	167.92	45.54	14.77 ± 2.22
175.13	61.10	10.30 ± 1.55	177.35	81.23	58.52 ± 9.69	175.65	53.27	10.81 ± 1.64
182.81	68.78	8.80 ± 1.34	185.14	89.02	44.63 ± 6.72	183.37	60.98	7.97 ± 1.20
194.34	80.31	6.70 ± 1.02	196.83	100.71	33.02 ± 4.96	194.94	72.55	5.43 ± 0.82
202.01	87.98	7.19 ± 1.11	204.61	108.49	28.73 ± 4.33	202.63	80.25	5.28 ± 0.80

average CN temperature for ER events decreases. One would therefore expect a narrower angular spread with increasing ER cross sections. This trend is in fact seen in Fig. 5 though the effect is found to be marginal.

IV. STATISTICAL MODEL CALCULATIONS

The experimental ER excitation functions were next compared with predictions from the statistical model of CN decay. The statistical model calculations were based on the assumption that the whole of the incident flux led to the CN formation, i.e., after capture, complete fusion between the target and the projectile was assumed while the possibility of NCN events was neglected [38]. The CN can decay into two major products, namely, the ER or the fission fragments along with the emission of light particles like neutrons, protons, α particles, and γ rays. While the particle and γ emission

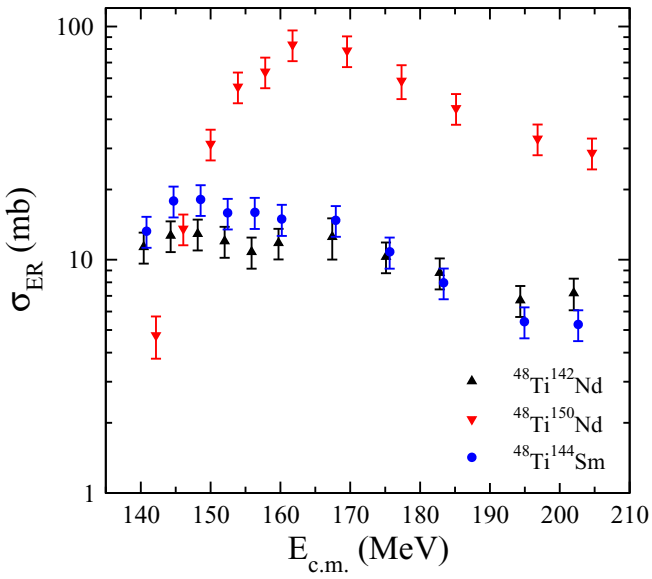

FIG. 4. ER cross sections for $^{48}Ti + ^{142,150}Nd$, ^{144}Sm systems as a function of $E_{c.m.}$.

widths were obtained from the Weisskopf formula as given in [39], the fission width was calculated from the transition-state theory of nuclear fission due to Bohr and Wheeler [40]. The Bohr-Wheeler fission width for a nucleus with total excitation energy E, measured, with respect to the ground-state mass of the CN, and angular momentum l is given as

$$\Gamma_f^{BW}(E,l) = \frac{1}{2\pi\rho_g(E^*)} \int_0^{E^*-B_f(l)} \rho_s[E^* - B_f(l) - \varepsilon]d\varepsilon, \quad (4)$$

where $E^\star$ is the intrinsic or thermal part of E and is given as $E^\star = E - E_{rot}(l) - E_{pair}$, with $E_{rot}(l)$ and E_{pair} being the rotational and pairing energies, respectively. The level densities at the ground state and the saddle configuration are denoted by ρ_g and ρ_s, respectively, and $B_f(l)$ is the angular-momentum-dependent fission barrier. Introducing the phase-space factor $\hbar\omega_g(l)/T$ to account for the collective degrees of freedom in the ground state [41], the fission width was obtained as

$$\Gamma_f(E,l) = \frac{\hbar\omega_g(l)}{T}\Gamma_f^{BW}(E,l), \quad (5)$$

Here $\omega_g(l)$ is the frequency of a harmonic oscillator potential having the same curvature of the nuclear potential at the ground state and T is the CN temperature.

The fission barrier $B_f(l)$ in the present calculation was obtained by incorporating the shell correction in the liquid-drop nuclear mass [42]. The shell correction term δ is given as the difference between the experimental and the liquid-drop model (LDM) masses ($\delta = M_{expt} - M_{LDM}$). The fission barrier then, is given as

$$B_f(l) = B_f^{LDM}(l) - (\delta_g - \delta_s), \quad (6)$$

where $B_f^{LDM}(l)$ is the angular-momentum-dependent LDM fission barrier and δ_g and δ_s are the shell correction energies for ground-state and saddle configurations, respectively. The LDM fission barrier was obtained from the finite-range rotating liquid-drop model (FRLDM) potential [43] and the ground-state shell corrections were taken from [44]. We further introduced a scaling factor K_f for the LDM fission barrier which was adjusted in order to reproduce the experimental ER

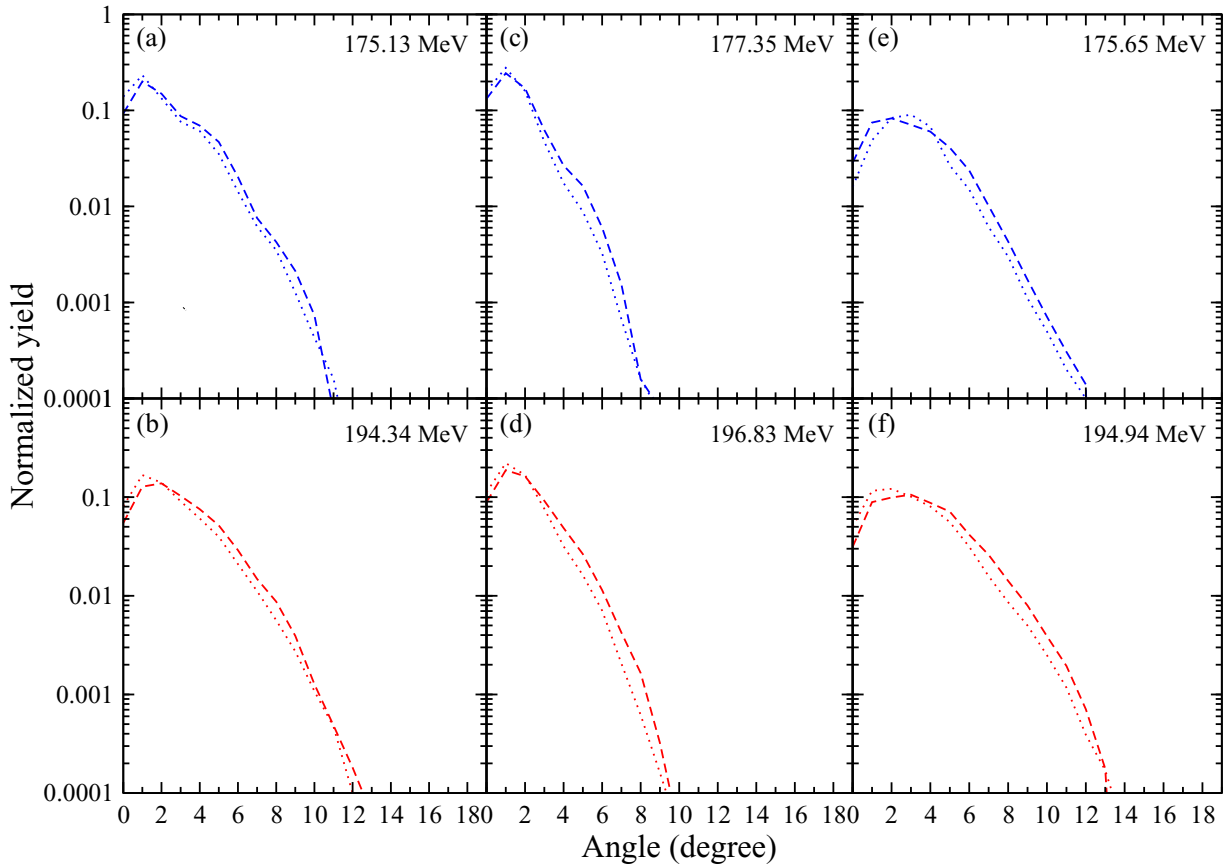

FIG. 5. ER angular distribution comparison with fission (dashed lines) and fission suppression (dotted lines) at two energy points for (a, b) ^{48}Ti + ^{142}Nd, (c, d) ^{48}Ti + ^{150}Nd, and (e, f) ^{48}Ti + ^{144}Sm systems obtained using statistical model calculations.

cross sections, and the following form of the fission barrier was used in the present work

$$B_f(l) = K_f B_f^{\mathrm{LDM}}(l) - (\delta_g - \delta_s). \tag{7}$$

For δ_g and δ_s, we used the prescription given in Ref. [45] for the deformation dependence of the shell correction, which yields a very small value of shell correction at large deformations and full shell correction at zero deformation. For small angular momentum of the CN, the fission barrier is high and the nuclear shape at the saddle is highly deformed and consequently, the shell correction at saddle deformation becomes negligible. However, with increasing angular momentum, the saddle configuration becomes more compact and for a large value of the angular momentum where the LDM fission barrier vanishes, the ground state and saddle configurations become infinitesimally close to each other. Consequently, the shell correction term in the fission barrier also vanishes in the above limiting condition.

The relative strengths of various decay modes of a CN depends on the density of levels of the parent and the daughter nuclei. The level density in turn is a sensitive function of the level density parameter (a), which was taken from the work of Ignatyuk *et al.* [46], who proposed the following form which includes shell effects at low excitation energies and goes over to its asymptotic form at high excitation energies:

$$a(E^*) = \tilde{a}\left(1 + \frac{f(E^*)}{E^*}\right)\delta, \tag{8}$$

with

$$f(E^*) = 1 - \exp(-E^*/E_D), \tag{9}$$

where $\tilde{a}$ is the asymptotic level density and E_D is a parameter which decides the rate at which the shell effects disappear with an increase in the intrinsic excitation energy ($E^\star$). A value of 18.5 MeV was used for E_D, which was obtained from an analysis of s-wave neutron resonances [47]. The shape-dependent asymptotic level density $\tilde{a}$ was taken from Ref. [47].

We next included the effect of the K degree (angular-momentum component of the CN along the symmetry axis) of freedom in fission width. The angular momentum of a CN can change its orientation from its initial direction along the perpendicular to the symmetry axis ($K = 0$) to nonzero values of K due to the coupling of the K degree of freedom with intrinsic nuclear motion [48]. Assuming a fast equilibration of the K degree of freedom, the fission width can be expressed as [49]

$$\Gamma_f(E,l) = \Gamma_f(E,l,K=0)\frac{K_0\sqrt{2\pi}}{2l+1}\mathrm{erf}\left(\frac{l+\frac{1}{2}}{K_0\sqrt{2}}\right), \tag{10}$$

where

$$K_0^2 = \frac{I_{\rm eff} T}{\hbar^2}, \tag{11}$$

and $I_{\rm eff} = \frac{I_\perp I_\parallel}{I_\perp - I_\parallel}$, $I_\perp$, and $I_\parallel$ being the moment of inertia at the saddle of the nucleus perpendicular to and about the nuclear symmetry axis. Here $\Gamma_f(E,l,K=0)$ denotes the fission width given in Eq. (5).

One of the important inputs to the statistical model calculation is the spin distribution of the fused system. We obtained the CN spin distribution from coupled-channel calculations using the CCFULL code [50] where the potential parameters were adjusted in order to fit the fusion excitation function. The projectile and target excited states used in the coupled-channel calculation are given in Table I. Using the CCFULL predicted CN spin distributions, we performed statistical model calculations with $K_{\rm f}$ as an adjustable parameter to reproduce the ER cross sections. Calculations were performed by both including and excluding shell effects in the level density and fission barrier. ER cross sections calculated with shell effects and for different values of $K_{\rm f}$ are compared with the experimental excitation function in Fig. 6. Statistical model predictions without considering shell effects are also shown in Fig. 7 along with the experimental ER cross sections.

V. DISCUSSION

It is observed from the experimental ER excitation functions that the ER cross sections for ^{48}Ti + ^{150}Nd forming ^{198}Pb are substantially larger than those of ^{48}Ti + ^{142}Nd and ^{48}Ti + ^{144}Sm systems forming ^{190}Pb and ^{192}Po, respectively, though the excitation energy of ^{198}Pb is higher than those of ^{190}Pb and ^{192}Po at the same center-of-mass energies on account of the difference between Q values of the reactions. The higher stability of ^{198}Pb against fission compared to ^{190}Pb and ^{192}Po can be attributed to the higher LDM fission barrier (11.90 MeV) of ^{198}Pb than those of ^{190}Pb and ^{192}Po (10.04 and 7.59 MeV, respectively) as well as to the higher shell correction energy (−5.08 MeV) of the former compared to the other two compound nuclei (−0.43 and 0.92 MeV, respectively). The above features are qualitatively reflected in the statistical model predictions for ER cross sections as shown in Figs. 6 and 7. However, a scaling factor for the LDM fission barrier is required to fit the experimental data. The calculated ER excitation functions for different values of the scaling factor are given in Fig. 6. While a reduction of the LDM fission barrier is found necessary to reproduce the experimental ER cross sections for the ^{48}Ti + ^{142}Nd and ^{48}Ti + ^{144}Sm reactions, fission barriers larger than the LDM barrier are required for the ^{48}Ti + ^{150}Nd reaction to fit the experimental data.

The best-fit values of the barrier scaling factor $K_{\rm f}$ obtained from statistical model calculations where shell correction is included both in the level density parameter and the fission barrier lie in the range (0.75–0.85) for the CN ^{190}Pb while the ranges for ^{198}Pb and ^{192}Po are (0.65–0.70) and (1.0–1.25), respectively. Without shell correction in statistical model calculation, the best-fit values of $K_{\rm f}$ lie in the ranges (0.75–0.85), (0.75–0.85), and (0.95–1.15) for the compound nuclei ^{190}Pb, ^{198}Pb, and ^{192}Po, respectively. The best-fit $K_{\rm f}$ values are shown in Fig. 8. It may be noted from Fig. 8 that shell correction does not make much difference in the scaling factor for ^{190}Pb on account of its small value. However, the shell correction decreases the best-fit values of $K_{\rm f}$ for ^{198}Pb and increases the same for ^{192}Po as expected from the nature of shell correction in the two nuclei (negative for ^{198}Pb and positive for ^{192}Po).

A barrier scaling to fit experimental ER cross sections was found necessary in a number of earlier works [4,5,21,51].

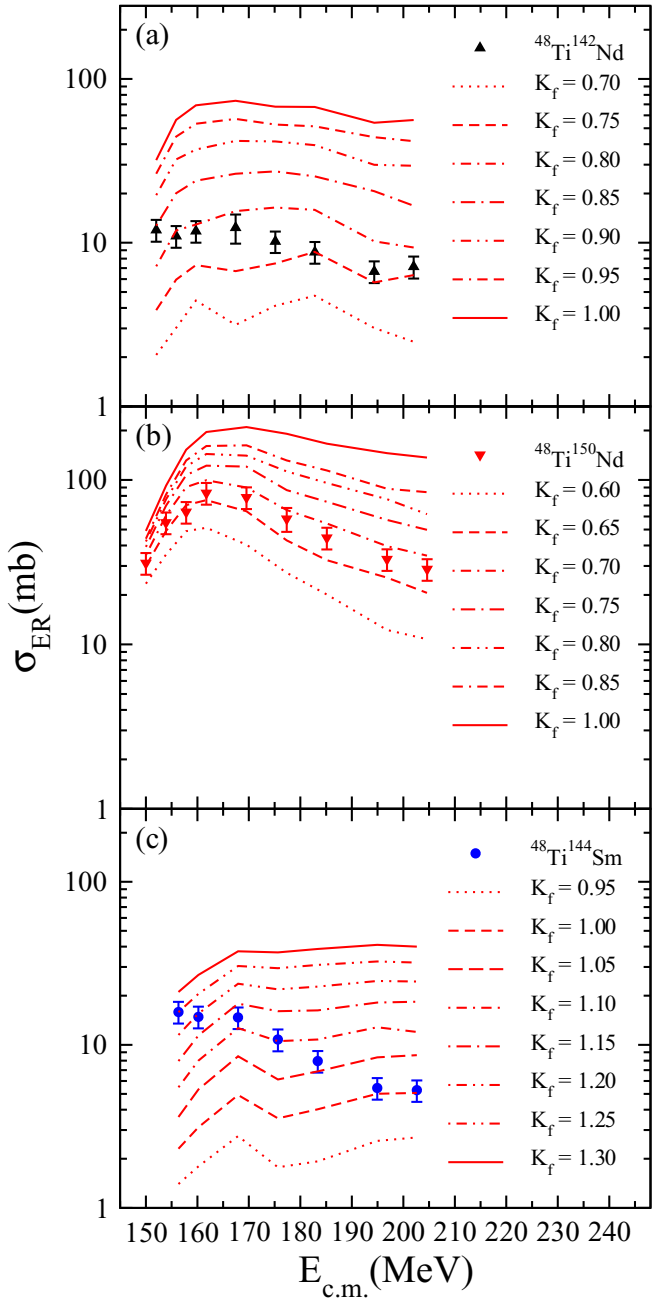

FIG. 6. Experimental ER cross sections (filled symbols) vs $E_{\rm c.m.}$ plotted with the theoretical results (various lines) obtained from the statistical model calculations after varying $K_{\rm f}$ values for (a) ^{48}Ti + ^{142}Nd, (b) ^{48}Ti + ^{150}Nd, and (c) ^{48}Ti + ^{144}Sm systems including the shell correction in the level density and the fission barrier.

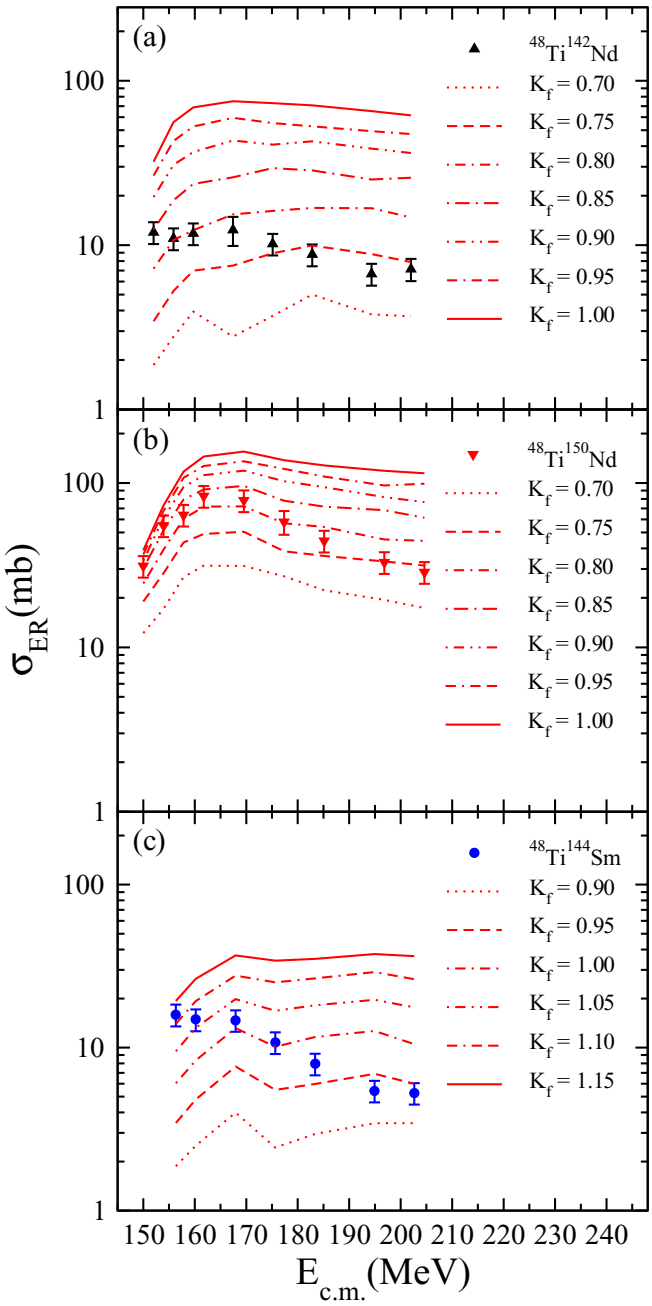

FIG. 7. Same as Fig. 6, but excluding the shell corrections.

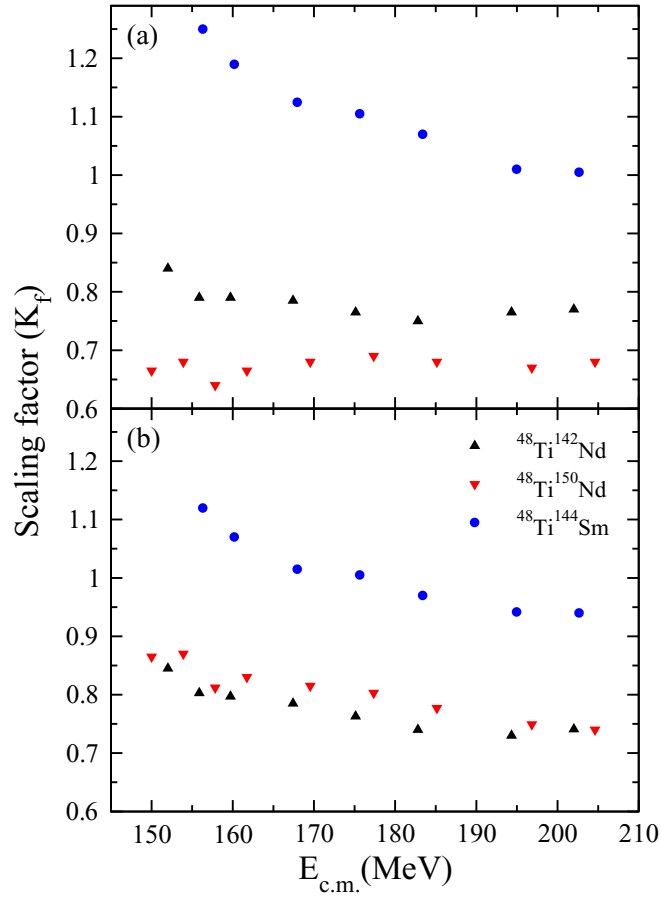

FIG. 8. Comparison of the best-fit values of K_f as a function of $E_{c.m.}$ using FRLDM fission barrier (a) including shell effects in the level density and fission barrier and (b) excluding shell corrections for ^{48}Ti + ^{142,150}Nd, ^{144}Sm systems.

Scaling factors less than 1 were reported for a number of Po isotopes populated through different (projectile + target) combinations [51]. Scaling factor values in the range (0.65–1.0) were required to fit experimental ER cross sections of ^{213,215,217}Fr isotopes formed in ^{19}F-induced reactions in the energy range of 82–122 MeV [5]. Mohanto *et al.* [4] also reported K_f values in the range (0.70–1.10) to fit the experimental ER cross sections of ^{30}Si,^{31}P + ^{170}Er systems in the energy range of 110–150 MeV. For the ^{48}Ti + ^{122}Sn system, barrier scaling factors in the range (0.65–1.0) were required [26].

Since statistical model calculations assume that the fusion probability of the target and projectile nuclei after capture is unity, overestimation of ER cross sections in comparison to experimental data can indicate that all capture events do not necessarily lead to complete fusion. Consequently, a barrier scaling factor less than unity can be interpreted as a signature of NCN processes [52]. Statistical model calculations for the present data therefore indicate the presence of NCN processes for the ^{48}Ti + ^{142}Nd and ^{48}Ti + ^{150}Nd reactions. However, statistical model results suggest no NCN process for the ^{48}Ti + ^{144}Sm reaction. A similar observation was also made in Ref. [7] where fission fragment mass distributions in the ^{48}Ca + ^{144}Sm reaction indicated no QF. However, it is observed from a comparison of the present results for the ^{48}Ti + ^{142}Nd forming the CN ^{190}Pb and ^{48}Ti + ^{144}Sm forming the CN ^{192}Po that though the statistical model predictions for ER cross sections for ^{190}Pb is about an order of magnitude higher than that for ^{192}Po due to shell closure of ^{190}Pb, their experimental values are comparable. This is surprising because the entrance-channel dynamics which decides the probability of CN formation is expected to be similar for the two reactions on account of their Q values being very close and both target nuclei being spherical. Further investigation to settle this issue is required possibly through the entrance-channel dynamical calculations to determine the CN formation probability as well as further improvements in the statistical model of CN decay.

VI. SUMMARY AND CONCLUSIONS

We have measured ER excitation functions for the ^{48}Ti + ^{142,150}Nd, ^{144}Sm systems over a broad range of beam energies. We have also performed a statistical model analysis of ER cross sections for these systems. The experimental ER cross sections of the ^{48}Ti + ^{150}Nd system are substantially higher than in the other two systems. The higher stability of ^{198}Pb formed in the ^{48}Ti + ^{150}Nd reaction can be traced to its larger LDM fission barrier as well as its larger shell correction energy compared to those of the CN formed in the other two reactions. Further, ER cross sections for both the ^{48}Ti + ^{142,150}Nd systems are much smaller than the statistical model predictions. This depletion of ER cross section suggests the presence of NCN processes in these two reactions.

A difference is, however, noted between the ^{48}Ti + ^{144}Sm and ^{48}Ti + ^{142}Nd systems since the statistical model predictions do not overestimate ER cross sections for the ^{48}Ti + ^{144}Sm system while it does so for the ^{48}Ti + ^{142}Nd system. Entrance-channel descriptions (Q values and target deformations) of these reactions being very similar, the above difference remains an open question.

ACKNOWLEDGMENTS

The authors thank the Pelletron + LINAC staff for providing a good quality beam during the whole experiment. The authors also acknowledge Abhilash S. R. of target laboratory of IUAC for their help and cooperation. The authors further thank Jhilam Sadhukhan of VECC, Kolkata, for providing the form factor of deformation-dependent shell corrections. P.S. acknowledges the financial assistance obtained from the University Grants Commission (UGC), Government of India. Financial assistance from UGC-DAE consortium for scientific research is also acknowledged.

[1] M. Dasgupta, D. J. Hinde, N. Rowley, and A. M. Stefanini, Annu. Rev. Nucl. Part. Sci. **48**, 401 (1998).
[2] M. Beckerman, Rep. Prog. Phys. **51**, 1047 (1988).
[3] E. Prasad, K. M. Varier, N. Madhavan, S. Nath, J. Gehlot, S. Kalkal, J. Sadhukhan, G. Mohanto, P. Sugathan, A. Jhingan, B. R. S. Babu, T. Varughese, K. S. Golda, B. P. Ajith Kumar, B. Satheesh, Santanu Pal, R. Singh, A. K. Sinha, and S. Kailas, Phys. Rev. C **84**, 064606 (2011).
[4] G. Mohanto, N. Madhavan, S. Nath, J. Gehlot, Ish Mukul, A. Jhingan, T. Varughese, A. Roy, R. K. Bhowmik, I. Mazumdar, D. A. Gothe, P. B. Chavan, J. Sadhukhan, S. Pal, Maninder Kaur, Varinderjit Singh, A. K. Sinha, and V. S. Ramamurthy, Phys. Rev. C **88**, 034606 (2013).
[5] V. Singh, B. R. Behera, M. Kaur, A. Kumar, K. P. Singh, N. Madhavan, S. Nath, J. Gehlot, G. Mohanto, A. Jhingan, I. Mukul, T. Varughese, J. Sadhukhan, S. Pal, S. Goyal, A. Saxena, S. Santra, and S. Kailas, Phys. Rev. C **89**, 024609 (2014).
[6] R. Sandal, B. R. Behera, V. Singh, M. Kaur, A. Kumar, G. Kaur, P. Sharma, N. Madhavan, S. Nath, J. Gehlot, A. Jhingan, K. S. Golda, H. Singh, S. Mandal, S. Verma, E. Prasad, K. M. Varier, A. M. Vinodkumar, A. Saxena, J. Sadhukhan, and S. Pal, Phys. Rev. C **91**, 044621 (2015).
[7] G. N. Knyazheva, E. M. Kozulin, R. N. Sagaidak, A. Yu. Chizhov, M. G. Itkis, N. A. Kondratiev, V. M. Voskressensky, A. M. Stefanini, B. R. Behera, L. Corradi, E. Fioretto, A. Gadea, A. Latina, S. Szilner, M. Trotta, S. Beghini, G. Montagnoli, F. Scarlassara, F. Haas, N. Rowley, P. R. S. Gomes, and A. Szanto de Toledo, Phys. Rev. C **75**, 064602 (2007).
[8] E. Prasad, K. M. Varier, R. G. Thomas, P. Sugathan, A. Jhingan, N. Madhavan, B. R. S. Babu, R. Sandal, S. Kalkal, S. Appannababu, J. Gehlot, K. S. Golda, S. Nath, A. M. Vinodkumar, B. P. Ajith Kumar, B. V. John, G. Mohanto, M. M. Musthafa, R. Singh, A. K. Sinha, and S. Kailas, Phys. Rev. C **81**, 054608 (2010).
[9] D. J. Hinde, M. Dasgupta, J. R. Leigh, J. P. Lestone, J. C. Mein, C. R. Morton, J. O. Newton, and H. Timmers, Phys. Rev. Lett. **74**, 1295 (1995).
[10] W. J. Swiatecki, Phys. Scr. **24**, 113 (1981).
[11] J. P. Blocki, H. Feldmeier, and W. J. Swiatecki, Nucl. Phys. A **459**, 145 (1986).
[12] A. M. Stefanini, M. Trotta, B. R. Behera, L. Corradi, E. Fioretto, A. Gadea, A. Latina, S. Szilner, Y. W. Wu, S. Beghini, G. Montagnoli, F. Scarlassara, A. Yu. Chizhov, I. M. Itkis, N. A. Kondratiev, I. V. Pokrovskiy, R. N. Sagaidak, G. N. Kniajeva, E. M. Kozulin, V. M. Voskressensky, S. Courtin, F. Haas, and N. Rowley, Eur. Phys. J. A **23**, 473 (2005).
[13] M. Trotta, A. M. Stefanini, L. Corradi, E. Fioretto, A. Gadea, S. Szilner, S. Beghini, G. Montagnoli, F. Scarlassara, A. Yu. Chizhov, I. M. Itkis, G. N. Kniajeva, E. M. Kozulin, N. A. Kondratiev, I. V. Pokrovsky, R. N. Sagaidak, V. M. Voskressensky, S. Courtin, O. Dorvaux, F. Haas, and N. Rowley, Nucl. Phys. A **734**, 245 (2004).
[14] B. B. Back, R. R. Betts, K. Cassidy, B. G. Glagola, J. E. Gindler, L. E. Glendenin, and B. D. Wilkins, Phys. Rev. Lett. **50**, 818 (1983).
[15] B. B. Back, Phys. Rev. C **31**, 2104 (1985).
[16] R. Rafiei, R. G. Thomas, D. J. Hinde, M. Dasgupta, C. R. Morton, L. R. Gasques, M. L. Brown, and M. D. Rodriguez, Phys. Rev. C **77**, 024606 (2008).
[17] R. G. Thomas, D. J. Hinde, D. Duniec, F. Zenke, M. Dasgupta, M. L. Brown, M. Evers, L. R. Gasques, M. D. Rodriguez, and A. Diaz-Torres, Phys. Rev. C **77**, 034610 (2008).
[18] A. C. Berriman, D. J. Hinde, M. Dasgupta, C. R. Morton, R. D. Butt, and J. O. Newton, Nature (London) **413**, 144 (2001).
[19] B. B. Back, P. B. Fernandez, B. G. Glagola, D. Henderson, S. Kaufman, J. G. Keller, S. J. Sanders, F. Videbæk, T. F. Wang, and B. D. Wilkins, Phys. Rev. C **53**, 1734 (1996).
[20] D. J. Hinde, M. Dasgupta, J. R. Leigh, J. C. Mein, C. R. Morton, J. O. Newton, and H. Timmers, Phys. Rev. C **53**, 1290 (1996).
[21] R. du Rietz, E. Williams, D. J. Hinde, M. Dasgupta, M. Evers, C. J. Lin, D. H. Luong, C. Simenel, and A. Wakhle, Phys. Rev. C **88**, 054618 (2013).
[22] A. Yu. Chizhov, M. G. Itkis, I. M. Itkis, G. N. Kniajeva, E. M. Kozulin, N. A. Kondratiev, I. V. Pokrovsky, R. N. Sagaidak, V. M. Voskressensky, A. V. Yeremin, L. Corradi, A. Gadea, A. Latina, A. M. Stefanini, S. Szilner, M. Trotta, A. M. Vinodkumar, S. Beghini, G. Montagnoli, F. Scarlassara, A. Ya. Rusanov, F. Hanappe, O. Dorvaux, N. Rowley, and L. Stuttgé, Phys. Rev. C **67**, 011603 (2003).

[23] C. J. Lin, R. du Rietz, D. J. Hinde, M. Dasgupta, R. G. Thomas, M. L. Brown, M. Evers, L. R. Gasques, and M. D. Rodriguez, Phys. Rev. C **85**, 014611 (2012).
[24] A. Wakhle, C. Simenel, D. J. Hinde, M. Dasgupta, M. Evers, D. H. Luong, R. du Rietz, and E. Williams, Phys. Rev. Lett. **113**, 182502 (2014).
[25] R. N. Sagaidak, G. N. Kniajeva, I. M. Itkis, M. G. Itkis, N. A. Kondratiev, E. M. Kozulin, I. V. Pokrovsky, A. I. Svirikhin, V. M. Voskressensky, A. V. Yeremin, L. Corradi, A. Gadea, A. Latina, A. M. Stefanini, S. Szilner, M. Trotta, A. M. Vinodkumar, S. Beghini, G. Montagnoli, F. Scarlassara, D. Ackermann, F. Hanappe, N. Rowley, and L. Stuttgé, Phys. Rev. C **68**, 014603 (2003).
[26] P. Sharma, B. R. Behera, S. Pal, and N. Madhavan, EPJ Web Conf. **86**, 00045 (2015).
[27] Y. T. Oganessian, V. K. Utyonkov, Y. V. Lobanov, F. S. Abdullin, A. N. Polyakov, I. V. Shirokovsky, Y. S. Tsyganov, G. G. Gulbekian, S. L. Bogomolov, B. N. Gikal, A. N. Mezentsev, S. Iliev, V. G. Subbotin, A. M. Sukhov, O. V. Ivanov, G. V. Buklanov, K. Subotic, M. G. Itkis, K. J. Moody, J. F. Wild, N. J. Stoyer, M. A. Stoyer, and R. W. Lougheed, Phys. Rev. C **62**, 041604 (2000).
[28] Y. T. Oganessian, V. K. Utyonkov, Y. V. Lobanov, F. S. Abdullin, A. N. Polyakov, I. V. Shirokovsky, Y. S. Tsyganov, G. G. Gulbekian, S. L. Bogomolov, B. N. Gikal, A. N. Mezentsev, S. Iliev, V. G. Subbotin, A. M. Sukhov, O. V. Ivanov, G. V. Buklanov, K. Subotic, M. G. Itkis, K. J. Moody, J. F. Wild, N. J. Stoyer, M. A. Stoyer, R. W. Lougheed, C. A. Laue, Y. A. Karelin, and A. N. Tatarinov, Phys. Rev. C **63**, 011301 (2000).
[29] D. Ackermann, S. Antalic, M. Axiotis, D. Bazzacco, S. Beghini, G. Berek, L. Corradi, G. De Angelis, E. Farnea, A. Gadea, F. P. Heßberger, S. Hofmann, M. G. Itkis, G. N. Kniajeva, E. M. Kozulin, A. Latina, T. Martinez, R. Menegazzo, G. Montagnoli, G. Münzenberg, Y. T. Oganessian, C. R. Alvarez, M. Ruan, R. N. Sagaidak, F. Scarlassara, A. M. Stefanini, S. Szilner, M. Trotta, and C. Ur, Eur. Phys. J. A **20**, 151 (2004).
[30] P. Sharma, S. R. Abhilash, B. R. Behera, N. Madhavan, and D. Kabiraj, in Proc. of the Int. Symp. on Nucl. Phys. **59**, 910 (2014).
[31] N. Madhavan, I. Mazumdar, T. Varughese, J. Gehlot, S. Nath, D. A. Gothe, P. B. Chavan, G. Mohanto, M. B. Naik, I. Mukul, and A. K. Sinha, EPJ Web Conf. **17**, 14003 (2011).
[32] S. Nath, A Monte Carlo code to model ion transport in dilute gas medium (unpublished).
[33] E. T. Subramanium, B. P. Ajith Kumar, and R. K. Bhowmik, CANDLE: Collection and Analysis of Nuclear Data using Linux Network http://www.iuac.res.in/NIAS (unpublished).
[34] S. Gil, F. Hasenbalg, J. E. Testoni, D. Abriola, M. C. Berisso, M. di Tada, A. Etchegoyen, J. O. Fernández Niello, A. J. Pacheco, A. Charlop, A. A. Sonzogni, and R. Vandenbosch, Phys. Rev. C **51**, 1336 (1995).
[35] A. Charlop, J. Bierman, Z. Drebi, A. Garcia, S. Gil, D. Prindle, A. Sonzogni, R. Vandenbosch, and D. Ye, Phys. Rev. C **51**, 628 (1995).
[36] S. Nath, Comput. Phys. Commun. **180**, 2392 (2009).
[37] A. Gavron, Phys. Rev. C **21**, 230 (1980).
[38] J. Sadhukhan and S. Pal, Phys. Rev. C **79**, 064606 (2009).
[39] P. Fröbrich and I. I. Gontchar, Phys. Rep. **292**, 131 (1998).
[40] N. Bohr and J. A. Wheeler, Phys. Rev. **56**, 426 (1939).
[41] V. M. Strutinsky, Phys. Lett. B **47**, 121 (1973).
[42] K. Mahata, S. Kailas, and S. S. Kapoor, Phys. Rev. C **92**, 034602 (2015).
[43] A. J. Sierk, Phys. Rev. C **33**, 2039 (1986).
[44] W. D. Myers and W. J. Swiatecki, Lawrence Berkeley Laboratory Report No. LBL-36803, 1994 (unpublished).
[45] W. D. Myers and W. J. Swiatecki, Nucl. Phys. **81**, 1 (1966).
[46] A. V. Ignatyuk, G. M. Smirenkin, and A. Tishin, Sov. J. Nucl. Phys. **21**, 255 (1975).
[47] W. Reisdorf, Z. Phys. A **300**, 227 (1981).
[48] J. P. Lestone and S. G. McCalla, Phys. Rev. C **79**, 044611 (2009).
[49] J. P. Lestone, Phys. Rev. C **59**, 1540 (1999).
[50] K. Hagino, N. Rowley, and A. T. Kruppa, Comput. Phys. Commun. **123**, 143 (1999).
[51] R. N. Sagaidak and A. N. Andreyev, Phys. Rev. C **79**, 054613 (2009).
[52] T. Banerjee, S. Nath, and S. Pal, Phys. Rev. C **91**, 034619 (2015).